Behavior of Sheared Granular Materials at Micro-Scale during the Cyclic Loading

Md. Mahmud SAZZAD[1,*]

[1]Department of Civil Engineering, Rajshahi University of Engineering & Technology, Rajshahi-6204, Bangladesh

*Corresponding Author: Md. Mahmud SAZZAD (Email: mmsruet@gmail.com)
(Received: 19-Nov-2021; accepted: 19-Apr-2022; published: 30-Jun-2022)
DOI: http://dx.doi.org/10.55579/jaec.202262.355

Abstract. *The aim of this paper is to explore the evolution of different micro-scale quantities during the cyclic loading using the discrete element method (DEM) for a granulate system such as sand. The numerical samples comprising of 9826 spheres were generated and consolidated isotropically using the periodic boundaries. These numerical samples were subjected to the cyclic loading for different maximum applied strains. The simulated stress-strain behavior was validated with the experiment and found an excellent agreement between them during loading and unloading. The evolutions of different micro-scale quantities were investigated in detail considering the variation of the maximum applied strain and the density of sample. It is noted that the evolution of the coordination number and the slip coordination number is a function of the maximum applied strain and the density of sample during the cyclic loading. The change of the slip coordination number is larger at the end of unloading than that at end of loading during the cyclic loading regardless of the values of the maximum applied strain and the density of sample. The ratio of strong contacts to all the contacts increases abruptly when the load is reversed, which is opposite to what is observed for the coordination number and the slip coordination number. The deviatoric fabric computed by the fabric tensor considering the strong contacts mimics the deviatoric stress irrespective of the values of the maximum applied strain and the density of sample during the cyclic loading. Moreover, a linear correlation between the macro and micro quantities exists regardless of the variation of the maximum applied strains or the variation of the density of the sample during the cyclic loading. The slopes of the lines of these correlations are almost same.*

Keywords

Micro-scale quantities, deviatoric fabric, cyclic loading, DEM.

1. Introduction

The granulate system such as sand is comprised of distinct particles and its behavior is very complex at micro-scale. The behavior of such granular materials at micro-scale has not yet been explained sufficiently. Laboratory based physical experiments such as the direct shear test and the triaxial test of granular materials suffer from poor reproducibility of the test samples and the restricted control of initial and boundary conditions. The boundary stress and strain can only be measured by using the traditional laboratory equipment and thus, the inherent physical processes remain unexplored. Indeed, several researchers inferred the micro-mechanics of the granulate systems such as sand [1]-[3]. However,

due to the lack of the comprehensive measurements of the micro-scale parameters and the related micro-mechanics, the quantitative conclusion related to the micro-scale mechanics is not completely accomplished.

DEM, on the other hand, contemplates the fundamental physical processes evolve during the shear in a granulate system and demonstrates to be a very useful and effective tool in modelling the discrete nature of a granulate system. The literature review reveals that DEM has been extensively used to explore the micro-mechanics of a granulate system such as sand. In most of the cases of the earlier studies, DEM is mainly used to simulate and explore the monotonic behavior of granular materials in two-dimension (2D) and three-dimension (3D) [4]-[14] and in a very few cases, it is used to explore the same for the cyclic loading [15]-[21]. For example, Ng and Dobry [15] simulated the behavior of granular materials for monotonic drained and undrained cyclic loading (constant volume) considering the disks and spheres by using the DEM and indicated that the simulated cyclic loading closely resembled the hysteresis loop formation and pore water pressure build up. Sitharam [16] simulated the drained and undrained cyclic loading considering the disks. Recently, Sazzad and Suzuki [17] investigated the influence of inherent anisotropic conditions on the micro-scale behavior of granular materials during the cyclic loading using the oval shaped particles for 2D DEM models and concluded that the change in fabric anisotropy is dominant for the first few loading-unloading cycles. Considering the variation of the confining pressure in a 2D dry granular sample, Sazzad [18] studied the effect of cyclic loading on the micro-scale behavior of granular materials using the DEM. Kuhn et al. [19] investigated the cyclic liquefaction behavior using the DEM by considering the octahedral particles which were comprised of the clusters of spheres. To predict the severity of a particular loading sequence, they proposed four scalar measures. The study depicted that the stress-based scalar measure exhibited the superior efficacy in predicting the initial liquefaction and pore pressure rise. Nevertheless, the studies mentioned above, simulated the macromechanical behavior qualitatively using the DEM for the cyclic loading.

The qualitative comparison of the simulated results obtained from the DEM studies with the laboratory experiment is valid as long as the behavior of granular materials at the micro level is of the major interest of the study. However, to validate the reliability of these micro-mechanical behaviors observed during the numerical simulation and to have more confidence in the micro-mechanical responses using the DEM, it is important that the simulated results by the DEM are compared with the experimental results quantitatively and then, the evolution of different micro-mechanical parameters including the fabric is explored. In spite of the fact, the quantitative comparison of the DEM results with the experimental result during the cyclic loading is rare in the literature. Among the earlier studies, only O'Sullivan et al. [20] reported a physical cyclic test using the dry Grade chrome steel balls under the vacuum confinement of 80 kPa and compared the experimental results with the DEM. Considering the limited number of such studies, it can be stated that more micro-scale behaviors should be explored to enhance our understanding during the cyclic loading. Thus, the primary objective of this study is to compare the simulated stress-strain response during loading and unloading by using the DEM under strain controlled condition with the experimental stress-strain response reported in O'Sullivan et al. [20] quantitatively. The major objective of the present study is to explore the evolution of different micro-scale parameters such as the coordination numbers and the deviatoric fabric during the cyclic loading for different maximum applied strains and densities of samples. The fabric was enumerated with the help of different fabric tensors defined based on the contact normal vectors. In this study, single micro-scale parameter based on the contact characteristic of the granular system is considered in contrast to considering many micro-scale parameters usually used in most other studies in the literature to establish a relationship between the macro and micro-scale quantities. The study reveals that a linear relationship between the macro and micro-scale quantities is possible considering a single micro-parameter during the

cyclic loading irrespective of the values of maximum applied strain and the density of sample.

2. Discrete element method

The discrete element method (DEM) is one of the family of numerical methods that is widely used for exploring the micro-scale behavior of granular materials. It is a versatile method for computing the motion of particulate media in different branches of science and engineering. DEM was originally proposed by Cundall and Strack [8] for modeling the discrete nature of granular materials. Each particle in DEM represents a separate grain which can translate and rotate independently through the interparticle contacts. A single particle can make many contacts and the contacts between particles can even break. Newton's second law of motion is used to compute the translational accelerations and rotational acceleration of a 3D particle that can be computed as follows:

$$m\ddot{x}_i = \sum F_i \qquad i = 1 - 3 \tag{1}$$

$$I\ddot{\theta} = \sum M \tag{2}$$

where F_i stands for force components, M stands for moment, m stands for mass, I stands for the moment of inertia, $\ddot{x}_i$ stands for the translation acceleration components and $\ddot{\theta}$ stands for the rotational acceleration of the particle. The accelerations are numerically integrated over a small time step to update particle velocities and positions. The associated equations are as follows:

$$x_i(t + \Delta t) = x_i(t) + \dot{x}_i(t)\Delta t \tag{3}$$

$$\dot{x}_i(t + \Delta t) = \dot{x}_i(t) + \ddot{x}_i(t)\Delta t \tag{4}$$

where $\dot{x}_i$ is the components of the velocity, x_i is the components of the position of the particle and Δt is the time step. The choice of the time step is of critical importance in DEM. The value of time step is chosen to be very small to ensure the overlaps to be very small. Otherwise, it may result unrealistic value of force. Suitable time step is approximated from Rayleigh surface wave propagation speed. Usually a fraction of this time step is taken to ensure the realistic force transmission rates and attain the numerical stability.

3. About the computer program OVAL

In this study, computer program OVAL [11] is used. It is a computer program written in FORTRAN language. The running of OVAL is available in both the Windows and Linux platform. It is used for modelling the discrete behavior of an assembly of particles using the DEM. OVAL has been recognized so far by many contributions in the literature and thus, its efficacy has been established [10, 11, 17, 18] [21]-[23]. In this study, Hertz-Mindlin contact model is used. The normal force of a Hertz-type contact is calculated as follows [24]:

$$F^n = \frac{\bar{E}a^3}{R_e} \tag{5}$$

$$\bar{E} = \frac{8G}{3(1-\nu)} \tag{6}$$

$$a = \sqrt{\frac{d \times R_e}{2}} \tag{7}$$

$$R_e = \frac{2R_1R_2}{R_1 + R_2} \tag{8}$$

Here, $\bar{E}$ represents the elastic constant, a represents the contact radius, d represents the overlap between the contacting particles, R_e represents the effective radius of curvature, R_1 and R_2 represent the radii of curvatures of two particles at contact.

4. Brief description of the physical cyclic test

In this study, the physical cyclic shear test reported by O'Sullivan et al. [20] on dry grade chrome steel balls under a vacuum confinement of 80 kPa was simulated. In the physical test, steel balls were considered to be an analogue of soil. The nonuniform sample in their study had three types of spheres having the radii of 2 mm,

2.5 mm and 3 mm, respectively. The mixing ratio of these spheres in the nonuniform sample was 1:1:1. The sample diameter was 101 mm and the height was 203 mm. The void ratio of the sample was 0.603. To prepare the sample, the latex membrane was sealed against the inside of a cylindrical mold using a vacuum. The characteristics of the spheres used in the cyclic test as reported in O'Sullivan et al. [20] have been summarized in Tab. 1. The particle to particle friction coefficient and the boundary to particle friction coefficient were computed by O'Sullivan et al. [25] and Cui [26]. For details of the physical test, readers are referred to O'Sullivan et al. [20].

Tab. 1: Characteristics of dry Grade chrome steel balls used in the cyclic test [20].

Properties	*Values*
Density of spheres (kg/m^3)	7.8×10^3
Shear modulus (Pa)	7.9×10^3
Poisson's ratio	0.28
Interparticle friction coefficient	0.096
Boundary friction coefficient	0.228

5. Preparation of numerical samples

5.1. Sample generation

Initially, a loose sample was generated in a parallelepiped as shown in Fig. 1 (height to width ratio of two) by using 9826 spheres randomly in such a way that a sphere cannot touch its neighbors. The radii of spheres were 2 mm, 2.5 mm and 3 mm similar to the physical test. The spheres were considered as particles because the physical test reported by O'Sullivan et al. [20] also considered dry grade chrome steel balls as analogue to soil. The mixing ratio of these spheres is 1:1:1 which is similar to O'Sullivan et al. [20]. It should be noted that the shape of the numerical sample is different from that of the physical test. It is expected that this difference has negligible impact on the overall results.

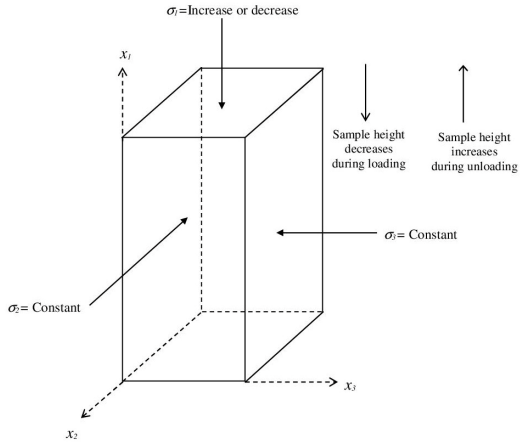

Fig. 1: Graphical illustration of the simulated model with reference axes.

5.2. Preparation of isotropically compressed sample

Once the sample was generation, it was consolidated in different stages to attain the target confining pressure of 80 kPa similar to the physical test. During the isotropic consolidation, the periodic boundary condition was applied similar to that used in many other DEM based studies [10, 11, 21, 27, 28]. A particle that sits astride a periodic boundary has a numerical image at the opposite boundary. If the centers of the particles move outside any boundary, they are instantly reintroduced at a corresponding position along the other boundary. The consolidation of the initially generated sparse sample was carried out in different stages using the strain controlled condition until the confining pressure became 80 kPa. When the confining pressure became 80 kPa, the isotropic compression was completed and the void ratio of the numerical sample became 0.626, which was very close to that reported in O'Sullivan et al. [20]. It should be noted that the void ratio of the isotropically consolidated numerical sample is a bit higher than that of the real sample. Such difference of the void ratio is believed to have negligible influence on the simulated results.

To prepare the isotropically compressed samples having different densities (i.e. void ratio) of sample, the interparticle friction coefficient

was intentionally turned off for the preparation of relatively dense sample and was 0.50 for the preparation of relatively loose sample. The sample was consolidated in different stages until the confining pressure became 80 kPa. The void ratio of the relatively dense sample became 0.58 and that of the relatively loose sample became 0.78 after the end of the isotropic consolidation.

5.3. Numerical simulation

Simulation of cyclic shear test was conducted using the isotropically compressed numerical samples for different maximum applied strains ranging from 0.1% to 2% and densities of sample by using the DEM. During the loading, the sample height was decreased downward with a very small strain increment of $2.0 \times 10^{-5}\%$ per time step along the x_1- direction by keeping the stresses in x_2- direction and x_3- direction constant (80 kPa). However, during the unloading, the process was reversed. The sample height was increased upward with the same strain increment along the x_1- direction by keeping the stresses in x_2- direction and x_3- direction constant (80 kPa). The cyclic loading condition of the simulated model is depicted in Fig. 1 for clarity.

To achieve the quasi-static condition and to minimize the effect of numerical damping, a very small strain increment was assigned. To examine the quasi-static condition of the sample during the simulation of cyclic loading, a non-dimensional index I_{uf} is used as follows [18, 21]:

$$I_{uf} = \sqrt{\frac{\sum_{1}^{N_p} F_{ubf}^2/N_p}{\sum_{1}^{N_c} F^2/N_c}} \times 100\,(\%) \qquad (9)$$

Here F_{ubf}, F, N_c, and N_p indicate the unbalanced force, contact force, number of contacts between particles and number of particles involved in the simulation, respectively. Index I_{uf} is directly linked to the accuracy of the simulation. Lower the value of I_{uf}, higher the accuracy of the simulation. An average value of I_{uf} below 2.0% is observed during the simulation of the cyclic loading. The material properties and DEM parameters used for the simulation of the cyclic loading are presented in Tab. 2.

Tab. 2: Material Properties and DEM parameters used in the present study.

Properties	*Values*
Density of spheres (kg/m^3)	7.8×10^3
Shear modulus (Pa)	7.9×10^3
Poisson's ratio	0.28
Interparticle friction coefficient	0.096
Increment of time step (s)	1.0×10^{-6}
Damping coefficients	0.10

5.4. Evolution of the simulated stress-strain responses

The stress-strain behavior simulated by using the DEM is compared with that of the physical cyclic test as reported in O'Sullivan et al. [20] and presented in Fig. 2. The stress ratio is defined here as $R_\sigma = (\sigma_1 - \sigma_3)/\sigma_3$. Here, σ_1 indicates the stress in x_1- direction and σ_3 indicates the stress in x_3- direction. Please note that half of the hysteresis loop of the simulated cyclic test is depicted in Fig. 2 to compare exactly with the experimental data. It is noted that the simulated stress-strain behavior by the DEM during loading and unloading has excellent agreement with the physical test reported in O'Sullivan et al. [20] under the strain controlled condition except the initial stiffening behavior. This may due to the difference in boundary conditions between the simulation and the experiment. This quantitative validation of the simulated stress-strain behavior with that of the experiment during loading and unloading depicts the versatile nature of the present study by DEM. It indicates that DEM can successfully reproduce the behavior of granular materials quantitatively. This quantitative validation of the numerical simulation by the DEM with the experiment during loading and unloading gives confidence about the authentication of the micro-scale responses reported in the following sections. After the quantitative validation of the simulated stress-strain behavior with the experiment, the effects of the variation of the maximum applied strain and the density of sample are studied. Figure 3 shows the effect of the variation of the maximum

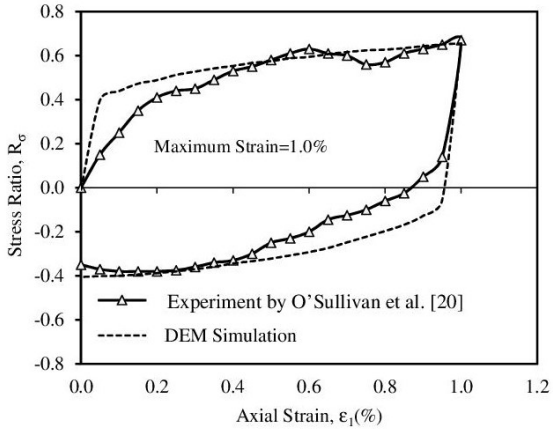

Fig. 2: Comparison of the simulated stress-strain behavior with that the experiment.

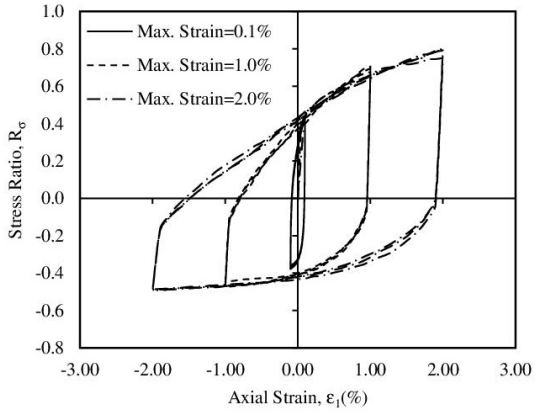

Fig. 3: Stress-strain response during the cyclic loading due to the variation of maximum applied strain.

applied strain on the stress-strain responses during the cyclic loading while Fig. 4 shows the effect of the variation of the density of sample on the stress-strain responses during the cyclic loading. The area covered by the hysteresis loop of the cyclic loading increases with the increase of the maximum applied strain (Fig. 3). Interesting to note that the sample having the void ratio of 0.78 becomes stiffer even at the second time loading (Fig. 4). Usually, this not expected for a relatively loose sample. However, this becomes possible because the interparticle friction coefficient is very small (0.096) during the cyclic shear which helps the loose sample to become denser sharply during the cyclic loading.

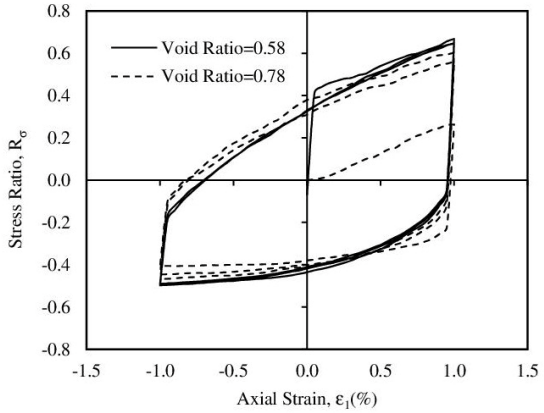

Fig. 4: Stress-strain response during the cyclic loading due to the variation of sample density for the 1% maximum applied strain.

5.5. Evolution of micro-scale behavior

In this section, the evolution of different micro-scale quantities such as the coordination number, slip coordination number, fabric and the relation between the fabrics and the stress ratio is discussed. The evolution of the coordination number with axial strain is depicted in Fig. 5. For clear representation, the coordination number for first loading and unloading (half of the hysteresis loop of cyclic loading) is depicted in Fig. 5-(a) while the same for few hysteresis loops of cyclic loading are depicted in Fig. 5-(b) for different maximum applied strains. The coordination number is usually defined as $Z = 2N_c/N_p$ [27, 28]. Two drops of coordination number are noticed in Fig. 5-(a). The first drop of coordination number is noticed when the isotropically compressed sample is subjected to loading and the second drop is noticed when the same sample is subjected to unloading. When the maximum applied strain is 0.10%, these drops are not as sharp as it is noticed in the case when the maximum strain is 1.0% and 2.0%, respectively. When the maximum strain is 0.10%, the contacts which are isotropically distributed start lining in parallel with the major principal stress direction and few contacts are lost in the minor principal stress directions. Consequently, the reduction of the coordination number is not so sharp during loading. When the load is re-

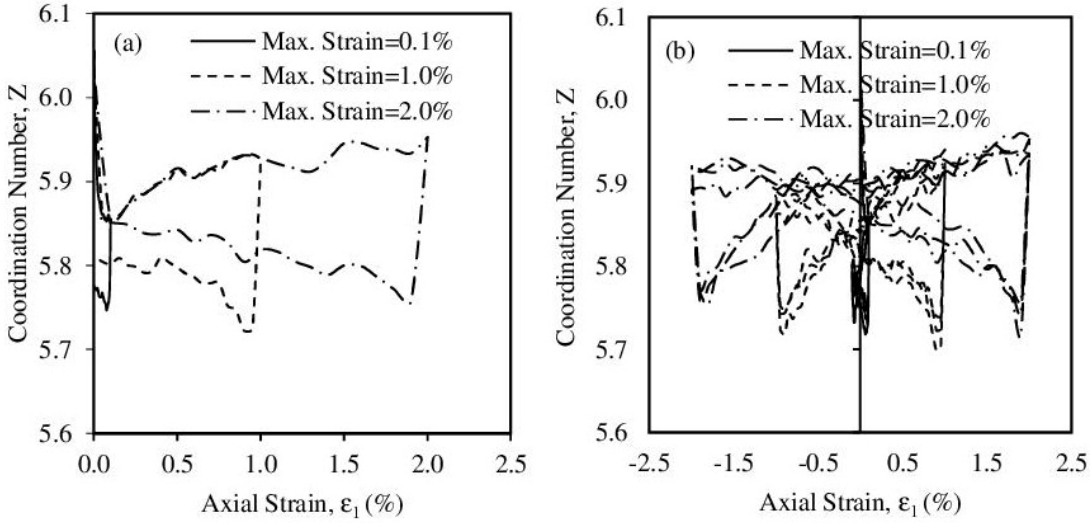

Fig. 5: Evolution of the coordination number with axial strain for different values of maximum applied strain: (a) for first loading and unloading and (b) for few cyclic loops.

versed, the principal stress direction is also inverted which causes the disintegration of few more contacts resulting in a second drop of coordination number. For the case when the maximum strain is as large as 2.0%, the sample gets enough time to redistribute the isotropically distributed contacts prior to shear and the contacts start lining in parallel with the direction of major principal stress by losing huge contacts in the directions of minor principal stress. When the loading continues, the number of contacts and the coordination number starts increasing again to support the accumulated force chains almost parallel to the direction of major principal stress. Similar mechanism takes place during unloading.

In the case of cyclic loading, another drop of coordination number is observed when the reloading begins as noted in Fig. 5-(b). This drop is also related to the redistribution of the contact fabric due to the change of the major principal stress direction. The behavior is similar regardless of the values of the maximum applied strain. The evolution of the coordination number with axial strain for different densities of samples is depicted in Fig. 6. As discussed earlier, relatively loose sample exhibits a huge drop of coordination number compared to the relatively dense sample as soon as the shear begins.

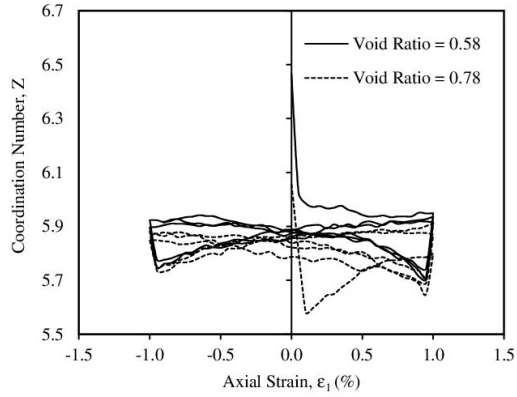

Fig. 6: Evolution of the coordination number with axial strain during the cyclic loading due to the variation of the sample density for 1% maximum applied strain.

The evolution of slip coordination number with axial strain during the cyclic loading for different values of maximum applied strain is depicted in Fig. 7. The slip coordination number is defined as $Z_{sl} = 2N_{sl}/N_p$ [27, 28], where N_{sl} indicates the total slip contacts among particles in the sample at a given state. Slip coordination number keeps increasing, on an average, till the

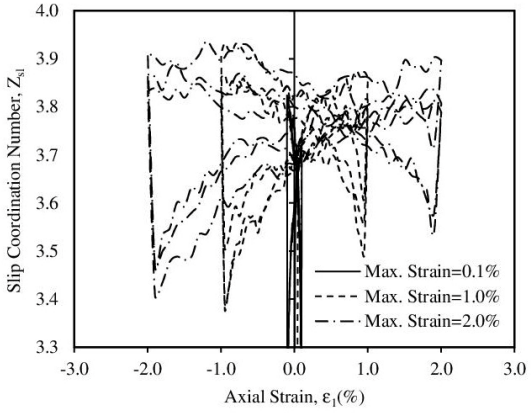

Fig. 7: Evolution of slip coordination number with axial strain during the cyclic loading for different values of the maximum applied strain.

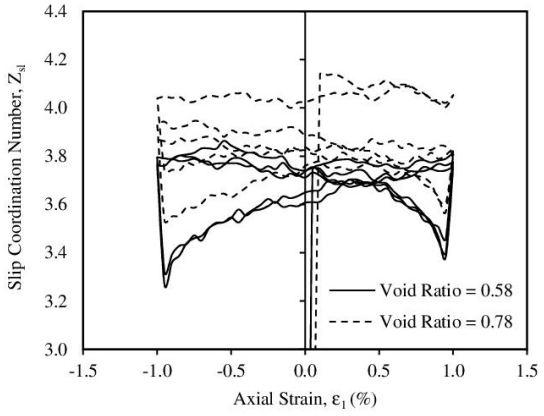

Fig. 8: Evolution of the slip coordination number with axial strain during the cyclic loading due to the variation of sample density for 1% maximum applied strain.

end of loading and experiences a huge drop when the load is reversed. The drop is due to the stress reversal to adjust the change in principal stress direction. The slip coordination number keeps increasing again as the unloading continues.

It should be noted that the evolution pattern of slip coordination number is similar regardless of the values of maximum applied strain. Note also that the drop of slip coordination number is larger at the end of unloading than that at end of loading. The evolution of slip coordination number with axial strain during the cyclic loading due to the variation of sample density for 1% maximum applied strain is showed in Fig. 8. The evolution pattern of slip coordination number is similar regardless of the variation of the sample density. As noted earlier, the drop of slip coordination number is larger at the end of unloading than that at end of loading.

The evolution of deviatoric fabric $H_{11} - H_{33}$ with axial strain (ε_1) considering all contacts during the cyclic loading for different applied strains is depicted in Fig. 9. The fabric is usually characterized by contact normal vectors [20, 21]. The fabric considering all contacts can be quantified in term of the contact normal vectors as follows [17, 18]:

$$H_{ij} = \frac{1}{N_c} \sum_{\alpha=1}^{N_c} n_i^\alpha n_j^\alpha \qquad i,j = 1-3 \qquad (10)$$

where n_i^α indicates the $i-$th component of the unit contact normal vector at the $\alpha-$th contact. A comparison of Fig. 9 with Fig. 3 shows that the evolution pattern of deviatoric fabric with axial strain follows almost the same tendency of stress-strain curve during the cyclic loading, even though the shape is different. The development of deviatoric fabric $H_{11} - H_{33}$ with axial strain (ε_1) considering all contacts during the cyclic loading for the variation of sample density for 1% maximum applied strain is shown in Fig. 10. A comparison of Fig. 10 with Fig. 4 shows that the evolution pattern of deviatoric fabric with axial strain considering the variation of the sample density follows almost the same tendency of stress-strain curve during the cyclic loading, even though the shape is different.

For representing the role of strong contacts and weak contacts in the evolution of fabric, the fabric considering all contacts can be divided into two different fabrics: (i) strong contact fabric considering the contact normal vectors at strong contacts only and (ii) weak contact fabric considering the contact normal vectors at weak contacts only [22]. In this study, a contact is defined as a strong contact if the contact force (F) between the contacting particles is greater than the average contact force (F_α). Similarly, a contact is defined as a weak contact if the contact force (F) between the contacting particles is smaller than or equal to the average

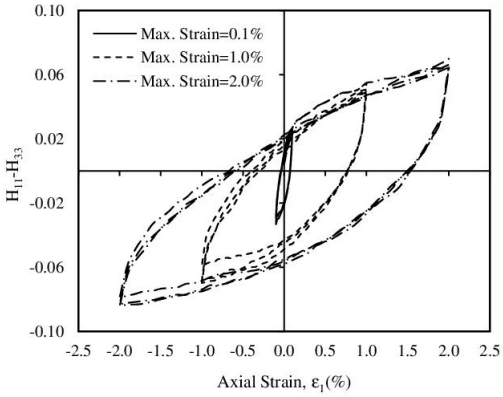

Fig. 9: Evolution of deviatoric fabric considering all contacts with axial strain during the cyclic loading for different values of maximum applied strain.

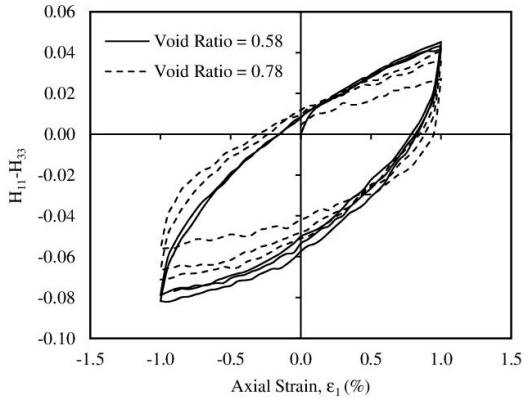

Fig. 10: Evolution of deviatoric fabric considering all contacts with axial strain during the cyclic loading due to the variation of sample density for 1% maximum applied strain.

contact force (F_α). The average contact force is described as follows:

$$F_\alpha = \sqrt{\frac{\sum_{k=1}^{N_c} |F^k|^2}{N_c}} \tag{11}$$

where F^k indicates the contact force at the $k-$th contact.

In this study, the ratio of strong contacts to all the contacts is represented by R and its evolution with axial strain is discussed to understand the role of strong contacts with respect to all the contacts. The evolution of R with axial strain during the cyclic loading is depicted in Fig. 11 for different values of maximum applied strain. Half of the hysteresis loop of the cycle loading is depicted in Fig. 11-(a) for clear view while few hysteresis loops of cyclic loading are depicted in Fig. 11-(b). The ratio of strong contacts to the total contacts decreases gradually except when $\varepsilon_1^{\max}$ is 0.10%. The value of R keeps decreasing as one can notice in Fig. 11 which is opposite to what is observed in the evolution of the coordination number. Although R reduces, the stress ratio at the same state of stress does not reduces, because these contacts carry heavy stress at these states. The value of R jumps up again immediate after the load reversal due to the sudden change of the principal stress direction. Later, R keeps reducing, on an average, during the unloading similar to the loading.

As strong contacts have considerable role in the evolution of micro-structures, the fabric tensor considering the strong contacts is defined similar to Eq. 8 as follows [17, 18]:

$$H_{ij}^s = \frac{1}{N_c} \sum_{s=1}^{N_s} n_i^s n_j^s \qquad i,j = 1-3 \tag{12}$$

where n_i^s represents the $i-$th component of the unit contact normal vector at the $s-$th strong contact and N_s represents the total number of strong contacts.

The evolution of the deviatoric fabric $H_{11}^s - H_{33}^s$ for different applied strains with axial strain (ε_1) during the cyclic loading is depicted in Fig. 12. The qualitative pattern of the evolution of fabric considering strong contacts is very close to the stress-strain curve during the cyclic loading compared to the evolution of fabric considering all contacts. The evolution of the deviatoric fabric $H_{11}^s - H_{33}^s$ for different densities of samples with axial strain (ε_1) during the cyclic loading is depicted in Fig. 13. It is noted that the qualitative pattern of the evolution of fabric considering strong contacts for different densities of samples is very close to the stress-strain curve during the cyclic loading compared to the evolution of fabric considering all contacts.

Because the evolution of $H_{11}^s - H_{33}^s$ with axial strain is similar to that of stress ratio with axial strain, it is envisioned to compare these re-

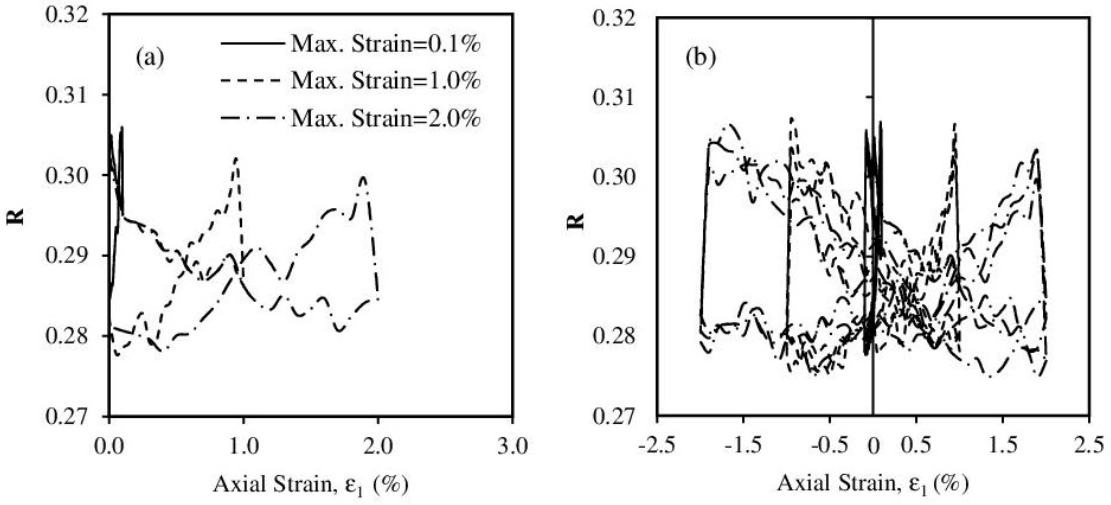

Fig. 11: Evolution of with axial strain for different values of maximum applied strain (a) during loading and unloading (b) during cyclic loading.

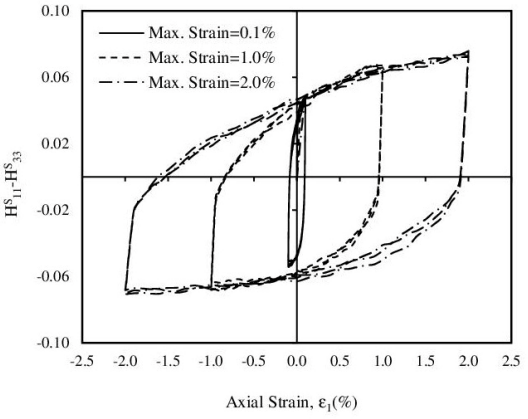

Fig. 12: Evolution of deviatoric fabric considering contact normal vectors at strong contacts with axial strain during the cyclic loading for different values of maximum applied strain.

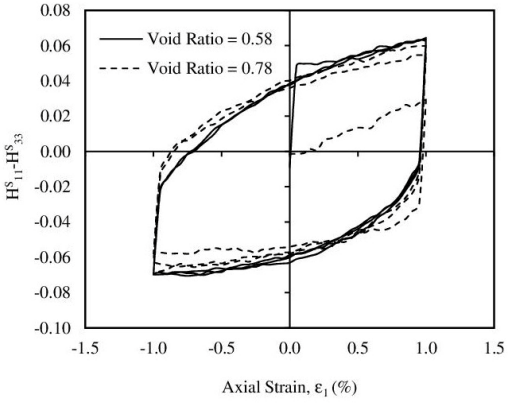

Fig. 13: Evolution of deviatoric fabric considering contact normal vectors at strong contacts with axial strain during the cyclic loading due to the variation of sample density for 1% maximum applied strain.

sults quantitatively. For this purpose, the deviatoric fabric for strong contacts during the cyclic loading is divided by H^s_{33} similar to stress ratio and depicted in Fig. 14. It is obvious from Fig. 14 that fabric ratio $[(H^s_{11} - H^s_{33})/H^s_{33}]$ computed by a fabric tensor of contact normal vectors at strong contacts can imitate the stress-strain behavior of granular material during the cyclic loading. This establishes an excellent connection between the macro quantity (stress ratio) and the micro quantity (fabric ratio) considering strong contacts. However, some mismatch between the simulated and experiment data is observed (Fig. 14). This may be due to the difference in the boundary conditions in the simulation and experiment. This study considers the

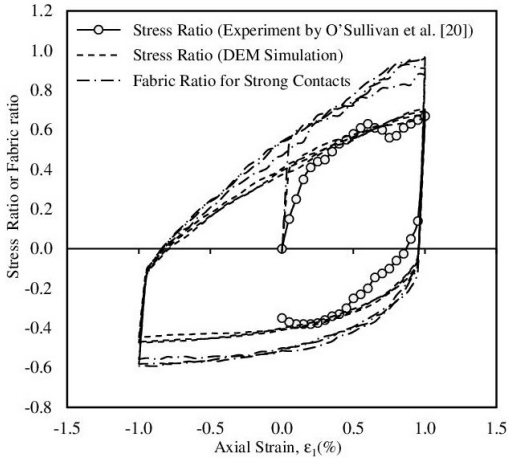

Fig. 14: Comparison of the simulated stress ratio or fabric ratio with the evolution stress ratio during the experimental cyclic test.

periodic boundary whereas the experiments by O'Sullivan et al. [20] used the flexible boundary.

As an excellent relation between the stress ratio and the fabric ratio considering the strong contacts during the cyclic loading is observed, a relationship between them can be developed. In the earlier studies, the relationship between the macro quantity such as the stress ratio and micro quantities regarding the contact normal vectors, normal stress and tangential stress was observed. In some studies, the relationship between the stress ratio and the anisotropies initiated from the contact normal vector, normal contact force and tangential contact force is established [29, 30]. By contrast, in this study, an attempt is made to correlate the stress ratio with the fabric ratio computed from the contact normal vectors of strong contacts during the cyclic loading [17, 18]. Only single micro-scale parameter related to the contact normal vectors is used in this approach. Consequently, this approach is simpler compared to the most other approaches in the literature. Figure 15 represents the correlation between the fabric ratio for strong contacts and stress ratio during the cyclic loading due to the variation of maximum applied strain and density of sample.

A linear correlation between the macro and micro quantity exists regardless of the values of

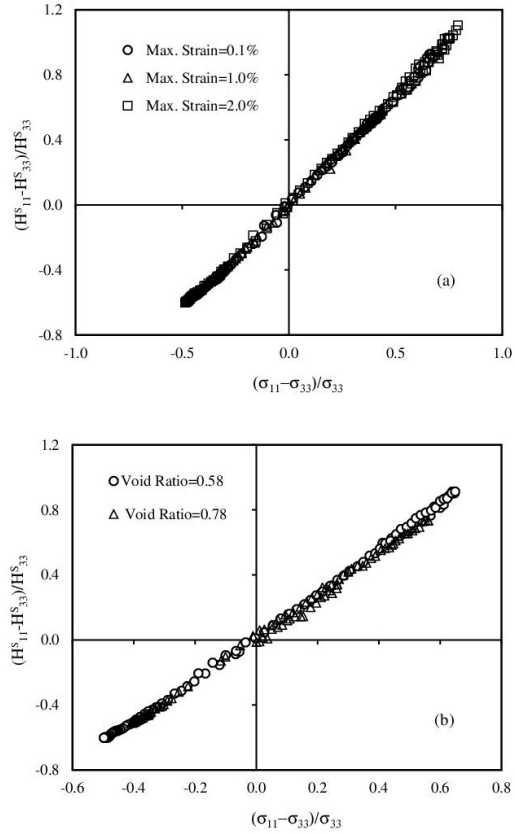

Fig. 15: The relationship between the micro-quantity (fabric ratio) and macro-quantity (stress ratio) during the cyclic loading (a) for different values of maximum applied strain (b) for different sample densities.

the maximum applied strain and density of sample during the cyclic loading. The correlation between the micro-quantity (fabric ratio) and macro-quantity (stress ratio) can be expressed as follows for the variation of the maximum applied strain (Eq. (13)) and for the variation of the density of the sample (Eq. (14)):

$$\left(\frac{H^s_{11} - H^s_{33}}{H^s_{33}}\right) = 1.32\left(\frac{\sigma_{11} - \sigma_{33}}{\sigma_{33}}\right) \qquad (13)$$

$$\left(\frac{H^s_{11} - H^s_{33}}{H^s_{33}}\right) = 1.34\left(\frac{\sigma_{11} - \sigma_{33}}{\sigma_{33}}\right) \qquad (14)$$

6. Conclusion

The simulated stress-strain response during the cyclic loading using the DEM is compared quantitatively with that of the experiment. In addition, the micro-mechanical responses during the cyclic loading are explored for different applied strains and densities of sample. The evolution of fabric during the cyclic loading is described and quantified using the fabric tensors considering all contacts and strong contacts. The major findings of this study are summarized as follows:

(i) The simulated drained cyclic behavior displays the similar stress-strain behavior as reported in the experiment except the initial stiffness of the stress-strain curve during the loading.

(ii) The evolution pattern of coordination number as well as slip coordination number is a function of the maximum applied strain and the density of sample during the cyclic loading.

(iii) The drop of slip coordination number is larger at the end of unloading than that at end of loading during the cyclic loading regardless of the values of maximum applied strain and the density of sample.

(iv) The ratio of strong contacts to all contacts increases abruptly as soon as the load is reversed which is opposite to what is observed for the coordination number and the slip coordination number.

(v) The deviatoric fabric considering the strong contacts mimics the deviatoric stress regardless of the values of maximum applied strain and the density of sample during the cyclic loading.

(vi) A linear correlation between the macro and micro quantity exists regardless of the values of maximum applied strain and the density of sample during the cyclic loading. The slopes of the lines of these correlation are almost same.

References

[1] Youd, T.L. (1977). Packing changes and liquefaction susceptibility. *Journal of the Geotechnical Engineering Division*, *103*(8), 918–922.

[2] Mitchell, J.K. (1993). *Fundamentals of Soil Behavior. 2nd Ed.* John Wiley & Sons New York.

[3] Chaudhary, S.K., Kuwano, J., Hashimoto, S., Hayano, Y., & Nakamura, Y. (2002). Effects of initial fabric and shearing direction on cyclic deformation characteristics of sand. *Soils and Foundations*, *42*(1), 147–157.

[4] Azéma, E., Radjai, F., Peyroux, R., & Saussine, G. (2007). Force transmission in a packing of pentagonal particles. *Physical Review E*, *76*(1), 011301.

[5] Azéma, E., Radjai, F., & Saussine, G. (2009). Quasistatic rheology, force transmission and fabric properties of a packing of irregular polyhedral particles. *Mechanics of Materials*, *41*(6), 729–741.

[6] Radjai, F., Wolf, D.E., Jean, M., & Moreau, J.J. (1998). Bimodal character of stress transmission in granular packings. *Physical review letters*, *80*(1), 61.

[7] Cui, L., O'sullivan, C., & O'neill, S. (2007). An analysis of the triaxial apparatus using a mixed boundary three-dimensional discrete element model. *Geotechnique*, *57*(10), 831–844.

[8] Cundall, P.A. & Strack, O.D. (1979). A discrete numerical model for granular assemblies. *geotechnique*, *29*(1), 47–65.

[9] Jiang, M., Yu, H.S., & Harris, D. (2005). A novel discrete model for granular material incorporating rolling resistance. *Computers and Geotechnics*, *32*(5), 340–357.

[10] Kuhn, M.R. (1999). Structured deformation in granular materials. *Mechanics of materials*, *31*(6), 407–429.

[11] Kuhn, M.R. (2003). Smooth convex three-dimensional particle for the discrete-element method. *Journal of Engineering Mechanics*, *129*(5), 539–547.

[12] Nouguier-Lehon, C., Cambou, B., & Vincens, E. (2003). Influence of particle shape

and angularity on the behaviour of granular materials: a numerical analysis. *International journal for numerical and analytical methods in geomechanics*, *27*(14), 1207–1226.

[13] Ng, T.T. (2001). Fabric evolution of ellipsoidal arrays with different particle shapes. *Journal of engineering mechanics*, *127*(10), 994–999.

[14] Oda, M., Nemat-Nasser, S., & Konishi, J. (1985). Stress-induced anisotropy in granular masses. *Soils and foundations*, *25*(3), 85–97.

[15] Ng, T.T. & Dobry, R. (1994). Numerical simulations of monotonic and cyclic loading of granular soil. *Journal of Geotechnical Engineering*, *120*(2), 388–403.

[16] Sitharam, T. *et al.* (2003). Discrete element modelling of cyclic behaviour of granular materials. *Geotechnical & Geological Engineering*, *21*(4), 297–329.

[17] Sazzad, M., Suzuki, K. *et al.* (2010). Micromechanical behavior of granular materials with inherent anisotropy under cyclic loading using 2D DEM. *Granular Matter*, *12*(6), 597–605.

[18] Sazzad, M.M. (2014). Micro-scale behavior of granular materials during cyclic loading. *Particuology*, *16*, 132–141.

[19] Kuhn, M.R., Renken, H.E., Mixsell, A.D., & Kramer, S.L. (2014). Investigation of cyclic liquefaction with discrete element simulations. *Journal of Geotechnical and Geoenvironmental Engineering*, *140*(12), 04014075.

[20] O'Sullivan, C., Cui, L., & O'NEILL, S.C. (2008). Discrete element analysis of the response of granular materials during cyclic loading. *Soils and Foundations*, *48*(4), 511–530.

[21] Sazzad, M.M. & Suzuki, K. (2011). Effect of interparticle friction on the cyclic behavior of granular materials using 2D DEM. *Journal of Geotechnical and Geoenvironmental Engineering*, *137*(5), 545–549.

[22] Sazzad, M.M., Azad, M.S., & Ghosh, A. (2022). Macro-and Micro-mechanical Responses of Granular Materials Under Different Stress Paths Using DEM. In *Advances in Civil Engineering*, Springer, 81–90.

[23] Sazzad, M., Shaha, R., Islam, M., & Kawsari, S. (2015). Macro and micro responses of granular materials under plane strain compression by 3D DEM. *Int J Adv Structs Geotech Eng*, *4*(2), 114–119.

[24] Sazzad, M., Sneha, E., & Rouf, R. (2017). Comparison of stress-stain behavior of CTC test using DEM simulation. In *International Conference on Planning, Architecture and Civil Engineering*, 194–199.

[25] Cui, L. (2006). *Developing a virtual test environment for granular materials using discrete element modelling*. Ph.D. thesis, University College Dublin Dublin, Ireland.

[26] O'Sullivan, C., Bray, J.D., & Riemer, M. (2004). Examination of the response of regularly packed specimens of spherical particles using physical tests and discrete element simulations. *Journal of engineering mechanics*, *130*(10), 1140–1150.

[27] Sazzad, M. (2016). Micro-scale responses of granular materials under different confining pressures using the discrete element method. *Acta Geotechnica Slovenica*, *13*(1), 27–36.

[28] Sazzad, M. *et al.* (2019). Effect of intermediate principal stress on the behavior of granular materials at a low mean stress by DEM. *Geotechnical and Geological Engineering*, *37*(5), 4539–4550.

[29] Rothenburg, L. & Bathurst, R. (1989). Analytical study of induced anisotropy in idealized granular materials. *Geotechnique*, *39*(4), 601–614.

[30] Ouadfel, H. & Rothenburg, L. (2001). Stress–force–fabric'relationship for assemblies of ellipsoids. *Mechanics of materials*, *33*(4), 201–221.

About Authors

Md. Mahmud SAZZAD is a professor in the Department of Civil Engineering of Rajshahi University of Engineering & Technology (RUET), Bangladesh. He received B.Sc. degree in Civil Engineering from Rajshahi University of Engineering & Technology in Bangladesh (2000), the M. Eng. degree in Civil Engineering from Saitama University, Japan (2006), and the Ph.D. degree in Civil Engineering from Saitama University, Japan (2011). He was the former head of the department of Urban & Regional planning, RUET. His current research interests include the discrete element method (DEM), Finite element method (1-.EM), computational mechanics, slope stability analysis, soil mechanics and foundation engineering, etc. Prof. Sazzad is the author/coauthor of more than 40 journal articles in renowned publisher including ASCE, Elsevier, Springer and 41 conference papers. He achieved Gold Medal Award for Outstanding Academic Performance in Bachelor of Science in Civil Engineering at RUET. He was a recipient of the ADB¬JSP Scholarship Program during his master degree and MEXT scholarship during his PhD degree. He is currently involved as the reviewer of many renowned International Journals and Conferences. He also worked as an Editor-in-Chief of International Journal of Advanced Structures and Geotechnical Engineering.